A Fluorinated Perylene Diimide for Green Solvent Processed Organic Solar Cell Cathode Interlayers

(Supporting Information)

Colton R. Atkinson[a], Rizwan Niazi[a], and Prof. Gregory C. Welch*[a]

[a] Department of Chemistry, University of Calgary, Calgary, Alberta, Canada T2N 1N4.

* Corresponding Author:

Email: gregory.welch@ucalgary.ca;

Phone Number: 1-403-210-7603

Table of Contents

1. Methods and Materials

Materials: Donor polymer (PM6) and small molecule acceptor Y6 were both purchased from Brilliant Matters. All other reactants, reagents, and solvents were purchased from Millipore-Sigma, VWR, or Combi-Blocks and used without further purification.

CHN Elemental Analysis: Elemental analyses were performed by Johnson Li in the Chemical Instrumentation Facility at the University of Calgary (UofC). A Perkin Elmer 2400 Series II CHN Elemental Analyzer was used to obtain CHN data, using ~1.5 mg of sample (with particle sizes ranging between 0.2 and 0.5 mm in diameter).

High-resolution MALDI-TOF (HR MALDI-TOF): High-resolution MALDI-TOF mass spectrometry measurements were performed by Johnson Li at the UofC. The sample solution (~ 1 µg mL-1 in dichloromethane) was mixed with matrix trans2-[3-(4-tert-Butylphenyl)-2-methyl-2-propenylidene]malononitrile (DCTB) solution (~5 mg mL-1 in methanol). All spectra were acquired using a Bruker Autoflex III Smartbeam MALDI-TOF, set to the positive reflective mode (Na:YAG 355 nm laser settings: laser offset = 62-69; laser frequency = 200 Hz; and number of shots = 300). The target used was Bruker MTP 384 ground steel plate target.

Nuclear Magnetic Resonance (NMR): All NMR spectroscopy experiments were recorded using a Bruker 500 MHz AVIII HD Spectrometer. All experiments were performed in $CDCl_3$. Chemical shifts (referenced to residual solvent) were reported in parts per million (ppm).

Cyclic Voltammetry (CV): All electrochemical measurements were performed using a Model 1200B Series Handheld Potentiostat by CH Instruments Inc. equipped with Ag wire, Pt wire and glassy carbon electrode, as the pseudo reference, counter electrode and working electrode respectively. Glassy carbon electrodes were polished with alumina. The cyclic voltammetry experiments were performed in anhydrous dichloromethane solution with ~0.1 M tetrabutylammonium hexafluorophosphate ($TBAPF_6$) as the supporting electrolyte at scan rate 100 mV/s. All electrochemical solutions were purged with dry N2 for 5 minutes to deoxygenate the system. Solution CV measurements were carried out with a small molecule concentration of ~0.2 mg/mL in dichloromethane. The ionization potentials (IP) and electron affinities (EA) were estimated by correlating the onsets of oxidation and reduction ($E_{ox}Fc/Fc^+$, $E_{red}Fc/Fc^+$) referenced to a ferrocene internal standard to that of the ionization potential of ferrocene using a conversion value of 4.8 (see: Advanced Materials, 1995, 7 (6), 551-554, Advanced Materials, 2011, 23 (20), 2367-2371).

UV-Visible Spectroscopy (UV-Vis): All optical absorption measurements were recorded using Agilent Technologies Cary 60 UV-Vis spectrometer at room temperature. Solution UV-Vis experiments were run in Heptane, Ethyl Acetate, Butanol, and Chloroform using 10 mm quartz cuvettes. Films were spin-cast into Corning glass micro slides from solutions of heptane and ethyl acetate (2 mg/mL) and chloroform (10 mg/mL) at 1500 rpm and butanol (2 mg/mL) at 3000 rpm. Prior to use, glass slides were cleaned with soap and water, acetone, and isopropanol, and followed by UV/ozone treatment using a Novascan UV/ozone cleaning system.

Solubility Determination: To find the maximum solubility, calibration curves were completed for both PDIN-EH and F-PDIN-EH to determine the molar absorptivity of both in each of heptane, ethyl acetate, and butanol (***Figures S14-19***). Then, saturated solutions were prepared and shaken overnight before allowing each to settle and syringe filtering out the remaining undissolved particulate matter. The saturated solutions were then diluted by a known factor and UV-Visible absorption measurements were taken to determine the maximum concentrations via the Beer-Lambert Law at room temperature.

Photoluminescence (PL): All emission measurements were recorded in ambient conditions using an Agilent Technologies Cary Eclipse fluorescence spectrophotometer.

Device Fabrication: The solution preparation, spin, slot-die coating, thermal annealing, and device characterizations were carried out in ambient air. The patterned indium tin oxide (ITO) substrates were subjected to 20 minutes of sequential ultrasonication cycles in deionized water (DI), acetone, and isopropyl alcohol respectively. These substrates were blow-dried with pressurized air and then placed in an Ossila UV-ozone chamber for minutes to remove organic contaminants from the surface if any. Conventional OPV device architecture was used. PEDOT: PSS (Al 40083) was spin-coated at 4000rpm from its water suspension. It was annealed at 140^{o}C for 20 minutes. Individual solutions of polymer donor (PM6) and non-fullerene acceptor BTP-4F (Y6) were prepared in chloroform at concentrations of 14.6 mg/ml and 17.4 mg/ml respectively. These solutions were heated at 50 ^{o}C overnight before mixing in 1:1 v/v ratios (1:1.2 w/w). 0.5% V/v CN was added as a solvent additive. Blend solutions were shaken for 30 minutes prior to coating. BHJ films were spin-coated at 3500 rpm for 30 seconds. The films were annealed at 110 ^{o}C for 10 minutes in ambient air. All CILs were coated from 0.5 mg ml^{-1} concentration in various solvents at 4000rpm for 40 seconds. No further post-processing was carried out. PDI CILs were slot-die coated from heptane with a sheer speed of 20 cm/min and a solution injection rate of 50 µl/min. The substrate-to-die-head gap was 100 µm. The substrate temperature was kept at 30 °C. 100 nm silver (Ag) was thermally evaporated using the Angstrom evaporation system. The active area of the devices is 0.14 cm^2.

Solar cell device characterization: The device measurements were carried out in N2 purged glove box. A Keithley 2420 source measure unit and Newport solar simulator (Model: 92251A-1000) with an irradiation intensity of 100 mW/cm^2 were employed to record current-voltage characteristics. A standard silicon solar cell (Newport 91150V) was used to calibrate light intensity. Device metrics and statistics were determined from the average of fifteen devices.

Atomic force microscopy: AFM images were acquired using AFM workshop model TT-2 AFM. All the images were recorded with the tapping mode. The images were processed using Gwyddion.

Melting Point Determination: Melting point was determined by Electrothermal 1101D MelTemp apparatus at a ramp rate of 1°C per minute. Samples were prepared by packing a small amount of F-PDIN-EH into a closed end melting point capillary tube. The melting point range was obtained by the combination of five separate melting point determination trials.

2. Synthetic Details

PDIN-H, PDIN-EH, and Br-PDIN-EH were each synthesized according to previously published literature.[1]

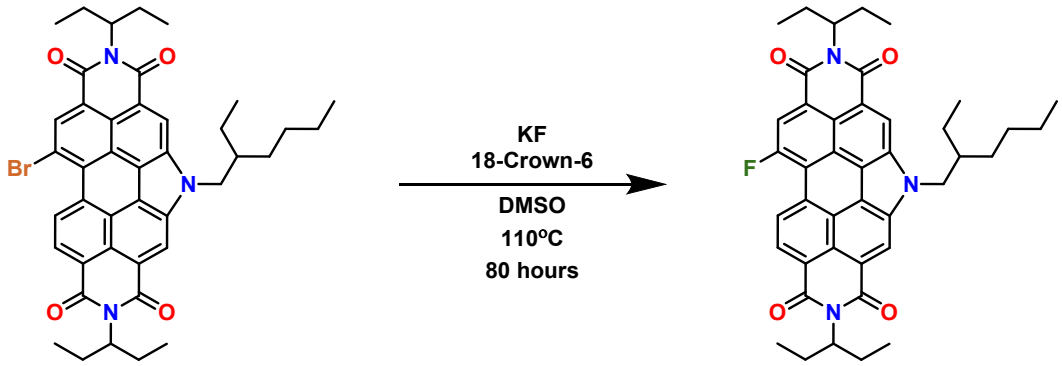

Synthesis of F-PDIN-EH:

Br-PDIN-EH (131mg, 0.18 mmol, 1.0 eq.), KF (136 mg, 2.34 mmol, 13 eq.), and 18-crown-6 (85 mg, 0.32 mmol, 1.8 eq.) were combined in a 20 mL glass pressure vial. The vial was sealed and purged with N_2 for 30 minutes. Then, 10 mL of dry, N_2 sparged DMSO was added. The vial was then placed into a LabArmor® bead bath at 110°C for 80 hours. The reaction mixture was then poured into water (100 mL) and stirred 20 minutes before vacuum filtration to obtain the crude red solid. The solid was then purified by silica gel column chromatography eluting with Hexane:EtOAc:CH_2Cl_2 (15:2:1). The organic solvent was removed by rotary evaporation and the resulting bright red film was redissolved into hot methanol. The methanol was then removed by rotary evaporation to give the pure F-PDIN-EH as a bright red powder. **Yield:** 40 mg (34%)

^{1}H NMR (500 MHz, $CDCl_3$) δ = 9.17 (d, $^3J_{H\text{-}H}$ = 8.1 Hz, 1H), 9.00 (s, 1H), 8.94 (s, 1H), 8.87 (d, $^3J_{H\text{-}H}$ = 8.1 Hz, 1H), 8.54 (d, $^3J_{H\text{-}F}$ = 12.1 Hz, 1H), 5.22 (dddd, *J* = 15.2, 11.4, 9.6, 5.9, 2H), 4.76 (h, *J* = 7.5, 2H), 2.36 (m, 5H), 2.02 (tddd, *J* = 13.4, 11.0, 7.4, 5.3, 4H), 1.38 (m, 9H), 0.98 (m, 15H), 0.85 (t, *J* = 7.3, 3H).

^{13}C NMR (126 MHz, $CDCl_3$) δ = 162.13, 160.05, 135.42, 135.09, 130.42, 128.52, 128.41, 124.44, 123.73, 123.66, 121.89, 121.36, 119.64, 119.30, 119.26, 119.14, 119.04, 58.16, 57.98, 51.17, 41.72, 30.97, 28.72, 25.38, 25.34, 24.41, 23.15, 14.11, 11.64, 11.61, 10.81.

^{19}F NMR (376 MHz, $CDCl_3$) δ = -105.02.

MALDI-TOF: m/z [M-2H]+H^+ expected: 672.3232 found: 672.3203

CHN: Theoretical (%) C: 74.86 H: 6.58 N: 6.24 Found (%) C: 74.84 H: 6.78 N: 6.07

Melting Point: 217-218°C

3. Processing Conditions of other Cathode Interlayer Materials in Literature

Table S1. The processing solvents of different CIL materials reported in literature.

CIL	Processing Solvent	Ref.
PDI-z	2,2,2-trifluoroethanol	[2]
PFN	Methanol	[3]
P(NDIDEG-T)	Water:Ethanol (36:64)	[4]
P(NDITEG-T)	Water:Ethanol (36:64)	[4]
PDINO-G	Ethanol	[5]
P1	2,2,2-trifluoroethanol	[6]
P2	2,2,2-trifluoroethanol	[6]
PDINN-F	Methanol	[7]
PDINN	Methanol	[8]
PDIN	Methanol	[8]
Alq_3-F1	Methanol	[9]
Alq_3-F2	Methanol	[9]
Alq_3-F3	Methanol	[9]
HBC-H	Ethanol	[10]
HBC-P	Ethanol	[10]
HBC-S	Ethanol	[10]
CTOC	2,2,2-trifluoroethanol	[11]
CTOC-N	2,2,2-trifluoroethanol	[11]
CTOC-N-Br	Methanol	[11]
PTPAPDINO	Methanol	[12]
PFN2TNDI	Methanol	[13]
NDI-M	2,2,2-trifluoroethanol	[14]
PDI-M	2,2,2-trifluoroethanol	[14]
PDI-NBr	Methanol	[15]
P1P-NBr	Methanol	[15]
P2P-NBr	Methanol	[15]
P3P-NBr	Methanol	[15]
P4P-NBr	Methanol	[15]
P1P-N	Methanol:Acetic Acid (97:3)	[15]
P2P-N	Methanol:Acetic Acid (97:3)	[15]
P3P-N	Methanol:Acetic Acid (97:3)	[15]
P4P-N	Methanol:Acetic Acid (97:3)	[15]
SiNCTI-N	Methanol	[16]
SiNCTI-NBr	Methanol	[16]
PDIEIE	Methanol	[17]
IIDPh-NSB	Methanol	[18]
IIDTh-PyBr	Methanol	[18]
IIDTh-NSB	Methanol	[18]

S1	Methanol	[19]
S2	Methanol	[19]
S3	Methanol	[19]
DPPN2TPA	Methanol	[20]
DPPM2TPA	Methanol	[20]
tPyDIN	Methanol	[21]
tPyDINO	Methanol	[21]
tPyDINBr	Methanol	[21]
FDPP2-N	Methanol	[22]
FDPP2-M	Methanol	[22]
PMI-TPP	Methanol, Ethanol, or Isopropanol	[23]
PMI-TMOPP	Methanol, Ethanol, or Isopropanol	[23]
OAS	Methanol	[24]
TOAS	Methanol	[24]
SAS	Methanol	[24]
PDI-PZ	2,2,2-trifluoroethanol	[25]
C_{60}-PZ	2,2,2-trifluoroethanol	[25]
PDIN-EH	Ethyl Acetate or Ethanol	[26,27]
F-PDIN-EH	Heptane, Ethyl Acetate or Butanol	**This work**

4. Mass Spectrometry and CHN Elemental Analysis

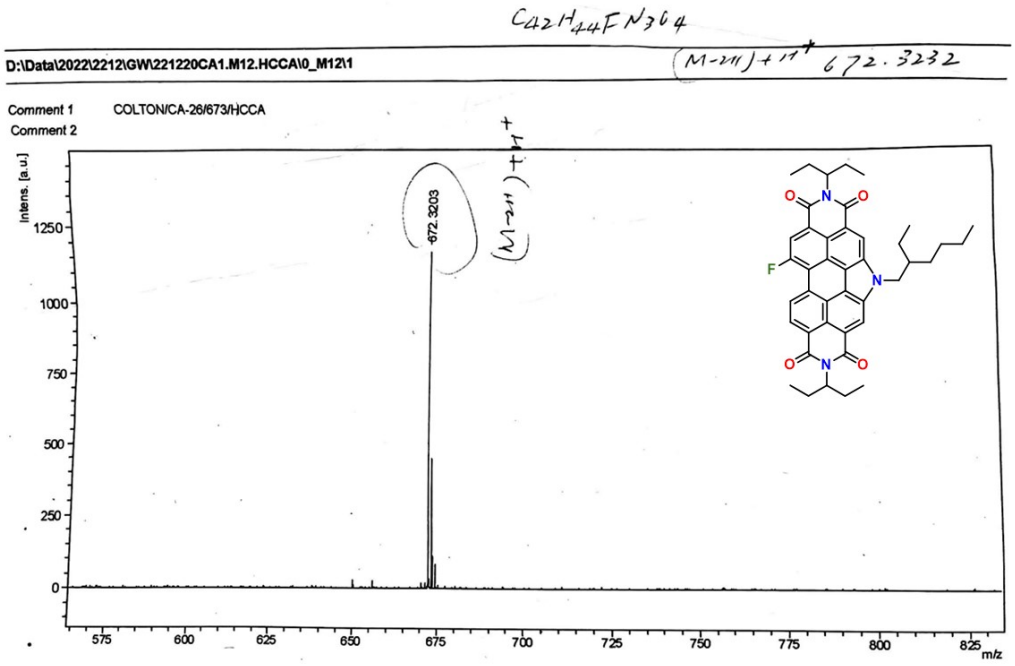

Figure S1: MALDI-TOF spectrum of **F-PDIN-EH**

University of Calgary
Department of Chemistry EA Date: 3-8-2023

Name:	COLTON	Group:	GW
Sample:	CA27-1	Weight (mg):	1.724
%C (Actual):	74.82	%C (Theorectical):	74.86
%H (Actual):	6.59	%H (Theoretical):	6.58
%N (Actual):	6.05	%N (Theoretical):	6.24
%S (Actual):	0.00	%S (Theoretical):	

Figure S2: CHN Elemental Analysis of **F-PDIN-EH**

5. ^{1}H, ^{13}C, and ^{19}F NMR Spectroscopies

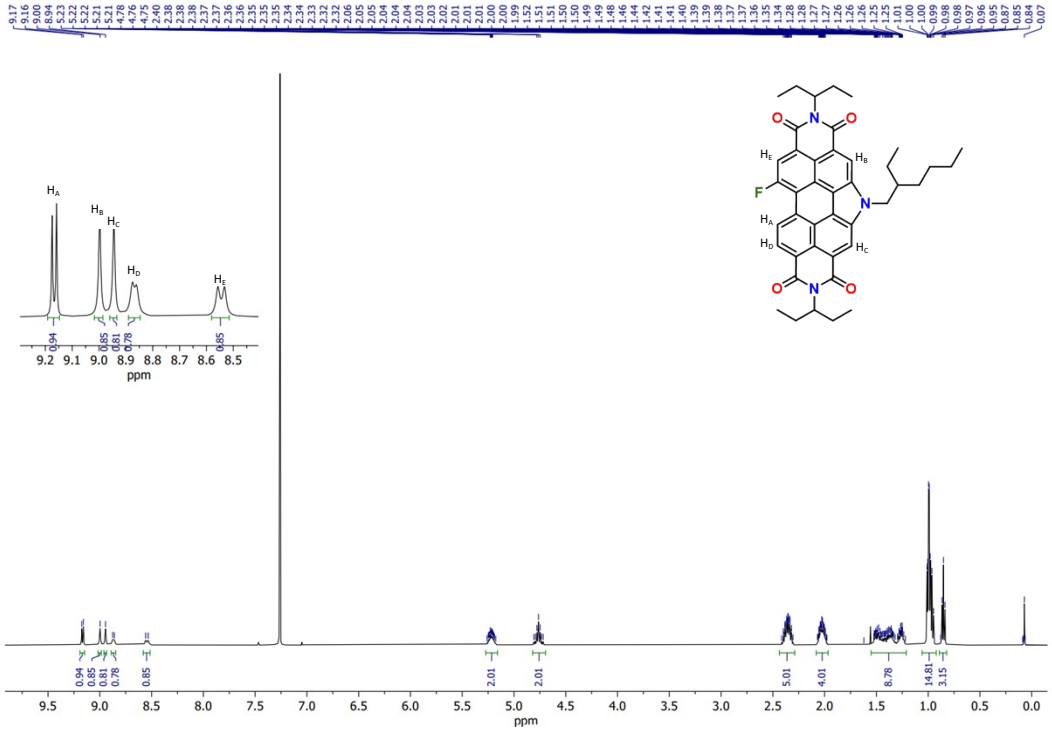

Figure S3 ^{1}HNMR spectrum of **F-PDIN-EH** (500 MHz, 295 K, $CDCl_3$)

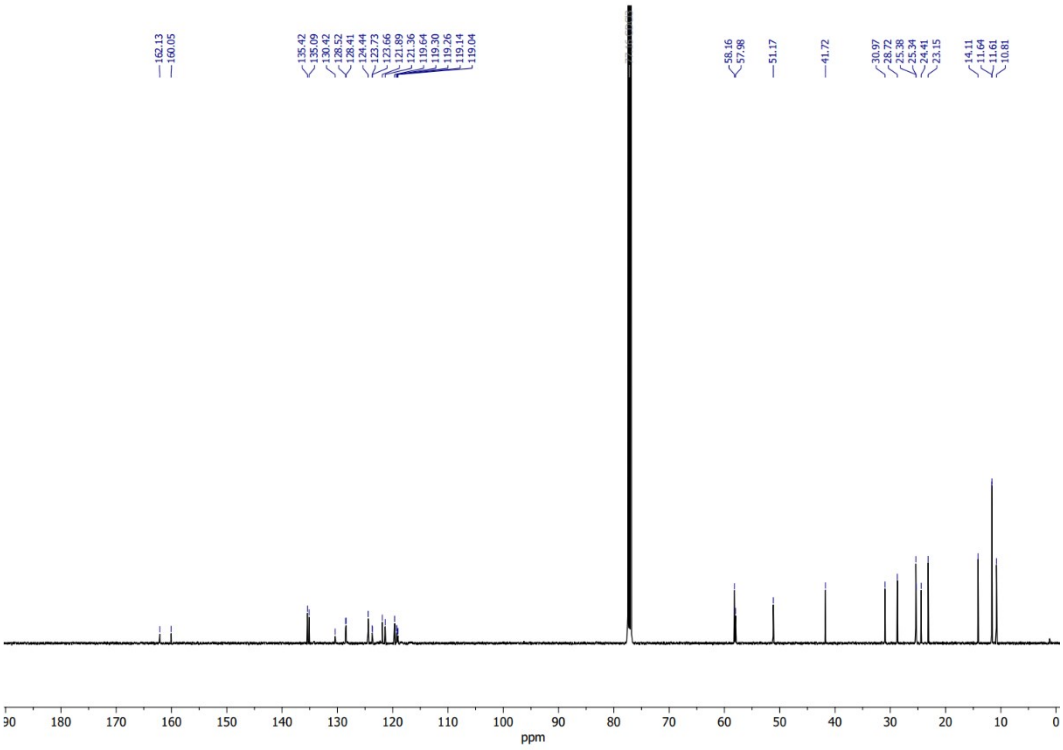

Figure S4 $^{13}C\{^{1}H\}$ NMR spectrum of **F-PDIN-EH** (126 MHz, 295 K, $CDCl_3$)

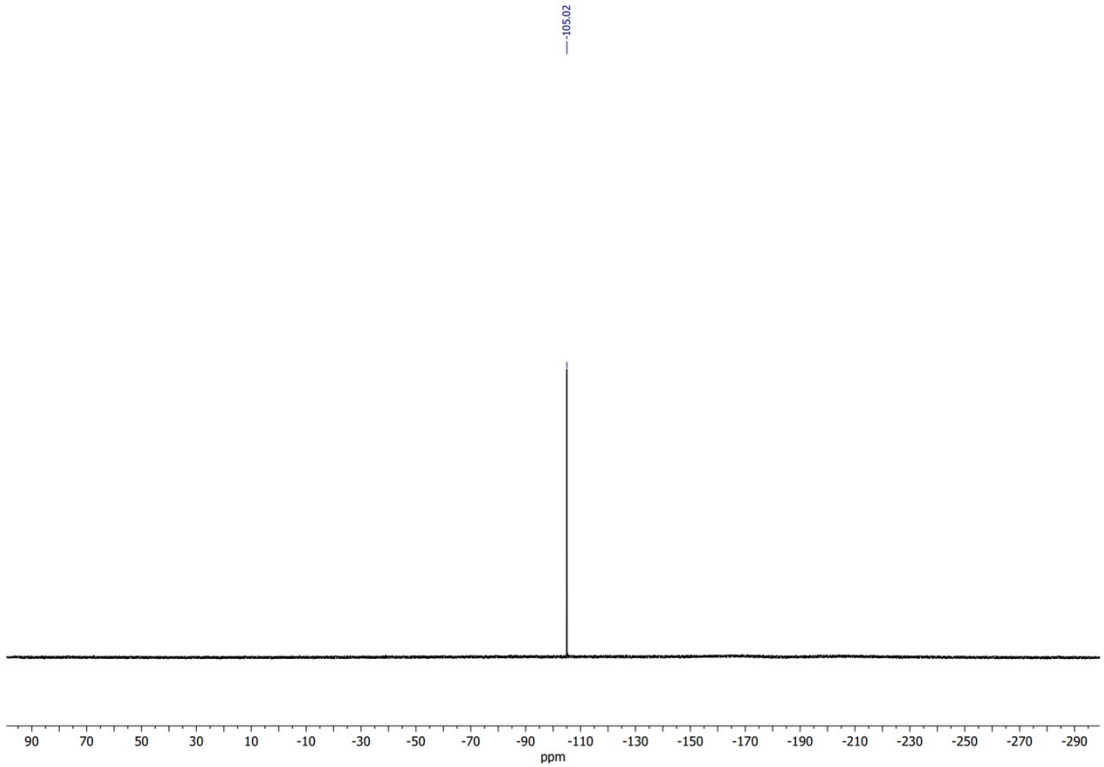

Figure S5 ^{19}F NMR Spectrum of **F-PDIN-EH** (376 MHz, 295 K, $CDCl_3$)

6. Comparing PDIN-EH and F-PDIN-EH Optical Absorption and Emission Spectra

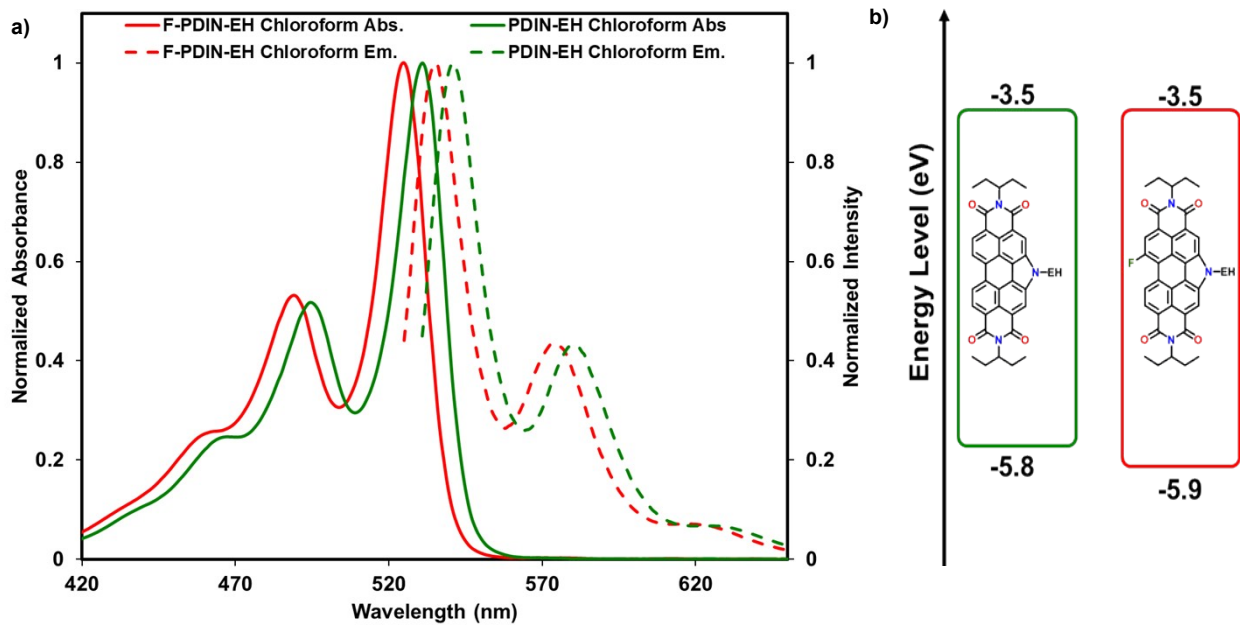

Figure S6: a) Solution UV-visible absorption and photoluminescence spectra of **PDIN-EH** and **F-PDIN-EH** in $CHCl_3$ taken in a 10 mm pathlength quartz cuvette (~10^{-5} M). $\lambda_{ex\ \textbf{F-PDIN-EH}}$: 525 nm, $\lambda_{ex\ \textbf{PDIN-EH}}$: 530 nm. b) The energy level diagram of **PDIN-EH** and **F-PDIN-EH** materials.

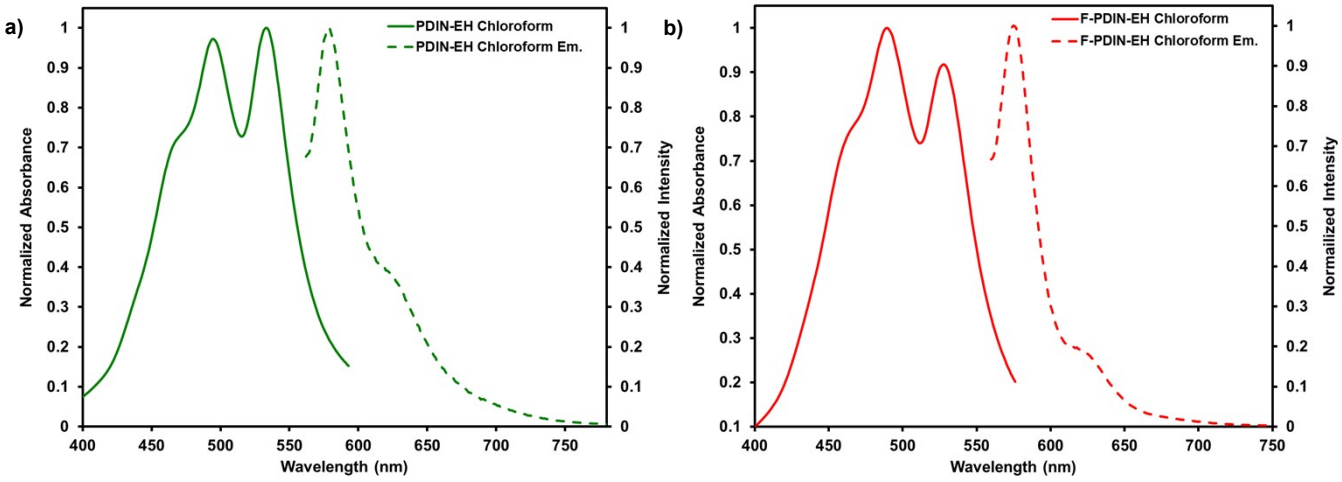

Figure S7: **a)** Optical absorption and photoluminescence spectra of **PDIN-EH** thin films spin cast from chloroform (10 mg/mL) onto glass substrates. $\lambda_{ex\ \textbf{PDIN-EH}}$: 533 nm. b) Optical absorption and photoluminescence spectra of **F-PDIN-EH** thin films spin cast from chloroform (10 mg/mL) onto glass substrates. $\lambda_{ex\ \textbf{F-PDIN-EH}}$: 528 nm.

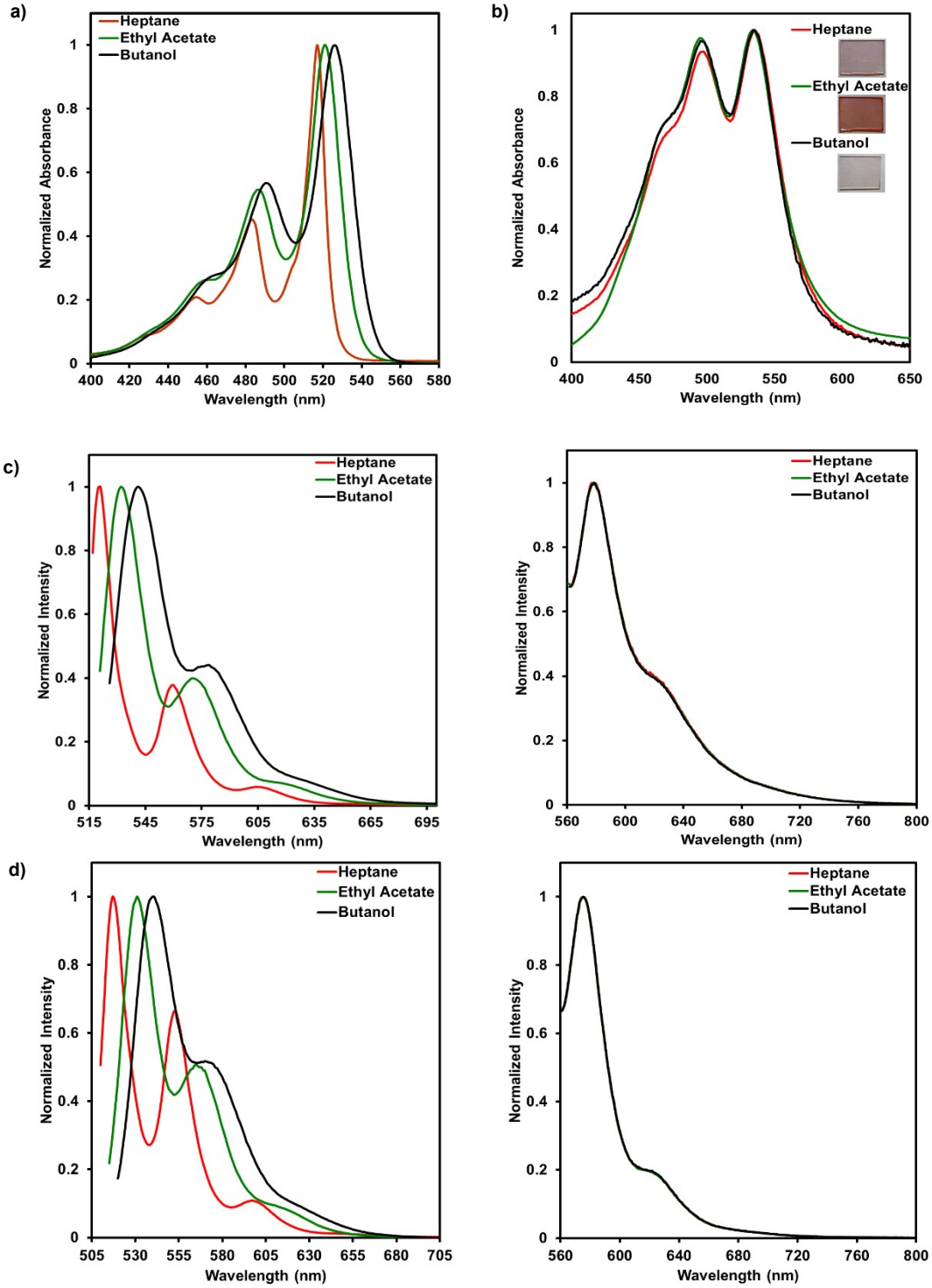

Figure S8. a) Normalized solution UV-visible absorption of **PDIN-EH** in heptane, butanol, and ethyl acetate.. b) Normalized thin film UV-visible absorption with inset images of the resulant films of **PDIN-EH** spin cast from heptane (2 mg/mL, 1000 rpm), ethyl acetate (2 mg/mL, 1000

rpm), and butanol (2 mg/mL, 3000 rpm). c) Normalized solution (left) and thin film (right) photoluminesnce spectra of **PDIN-EH** spin cast from heptane (2 mg/mL, 1000 rpm), ethyl acetate (2 mg/mL, 1000 rpm), and butanol (2 mg/mL, 3000 rpm) d) Normalized solution (left) and thin film (right) photoluminesnce spectra of **F-PDIN-EH** spin cast from heptane (2 mg/mL, 1000 rpm), ethyl acetate (2 mg/mL, 1000 rpm), and butanol (2 mg/mL, 3000 rpm).

Table S2. A comparison of the photophysical properties of **PDIN-EH and F-PDIN-EH** in solution.

Interlayer	Solvent	$\lambda_{max\ abs}$ (nm)	λ_{edge} (nm)	$\lambda_{max\ em.}$ (nm)	Stoke's Shift (cm^{-1})	$\varepsilon_{solution}$ ($M^{-1}\ cm^{-1}$)	Ehancement to Solubility
PDIN-EH	Heptane	517	527	521	148.5	150,500	-
	Ethyl Acetate	521	539	532	396.9	203,000	-
	Ethanol	526	546	541	527.1	124,000	-
	Butanol	524	545	541	599.7	120,000	-
F-PDIN-EH	Heptane	511	521	517	227.1	147,400	9.2X
	Ethyl Acetate	516	534	531	547.5	238,600	1.8X
	Ethanol	520	541	540	712.3	140,000	1.9X
	Butanol	518	541	540	786.5	227,700	1.3X

Table S3. The Hansen Solubility Parameter Determination for **F-PDIN-EH** and **PDIN-EH**.

Solvent	Solvating Ability F-PDIN-EH	Solvating Ability PDIN-EH
Acetone	Good	Good
Acetonitrile	Bad	Bad
1-Butanol	Good	Bad
t-Butyl Alcohol	Bad	Good
Chloroform	Good	Good
Cyclohexane	Good	Good
Cyclohexanone	Good	Good
Diethyl Ether	Good	Good
Diethylene Glycol Monoethyl Ether	Good	Bad
Dimethyl Sulfoxide (DMSO)	Bad	Bad
1,4-Dioxane	Good	Good
Ethanol	Bad	Bad
Ethyl Acetate	Good	Good
Ethyl Lactate	Good	Good
Ethylene Glycol	Bad	Bad
Ethylene Glycol Dimethyl Ether	Good	Good
Heptane	Good	Bad
Hexane	Good	Bad
Isophorone	Good	Good
d-Limonene	Good	Good
Methanol	Bad	Bad
Methyl Cellosolve (2-methoxyethanol)	Bad	Bad
Methyl Ethyl Ketone (MEK) (2-butanone)	Good	Good
N-Methyl-2-Pyrrolidone (NMP)	Good	Good
Methylene Chloride	Good	Good
N,N-Dimethyl Acetamide	Good	Good
N,N-Dimethyl Formamide (DMF)	Good	Good
Propylene Carbonate	Bad	Bad
Sulfolane (Tetramethylene Sulfone)	Bad	Bad
Tetrahydrofuran (THF)	Good	Good
Toluene	Good	Good
Xylene	Good	Good

7. Concentration Dependent Optical Absorption Plots

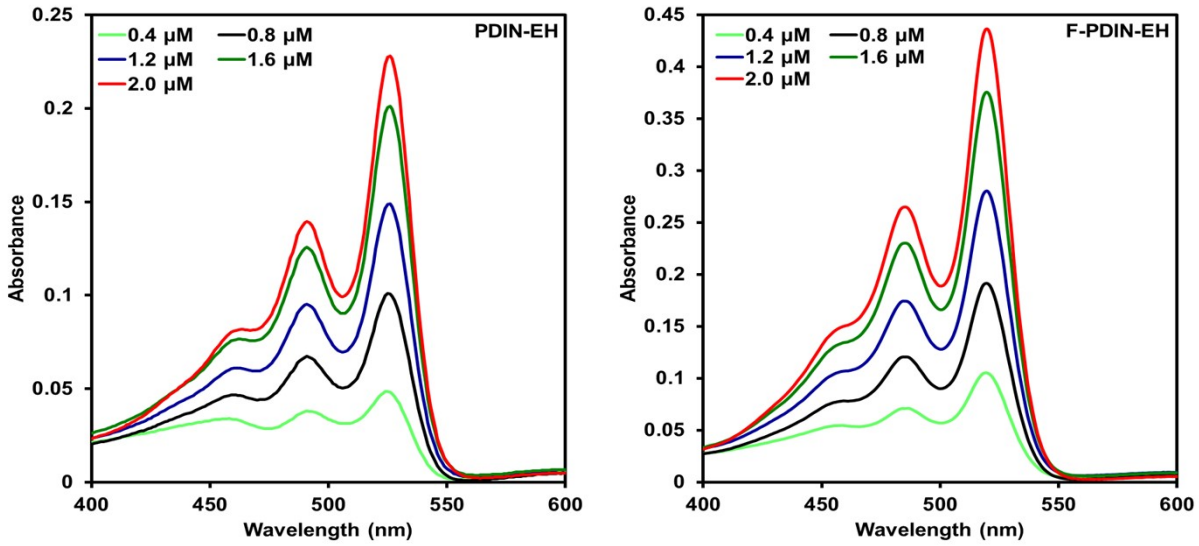

Figure S9: UV-Visible Absorption spectra for **PDIN-EH** (left) and **F-PDIN-EH** (right) material in butanol at 0.4 to 2.0 µM concentrations taken in a 10mm pathlength quartz cuvette. λ_{max} **PDIN-EH**: 526 nm λ_{max} **F-PDIN-EH**: 520 nm.

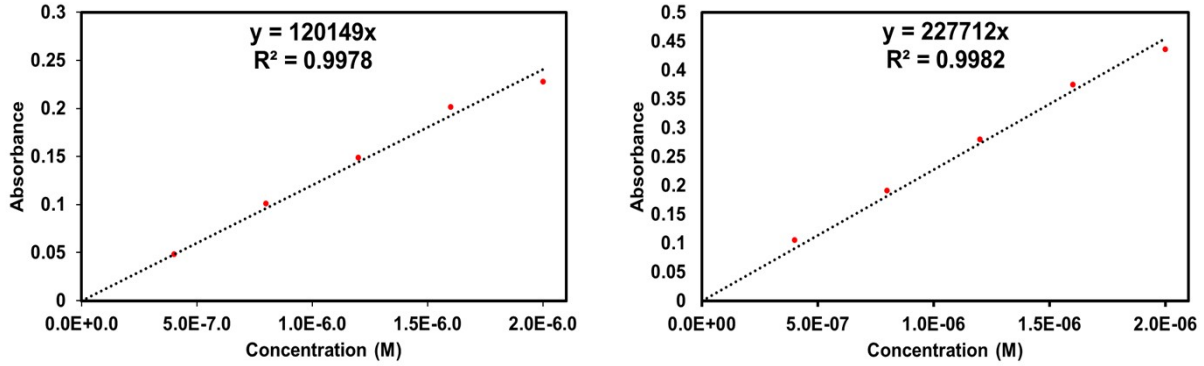

Figure S10: Absorbance vs Concentration plots for **PDIN-EH** (left) and **F-PDIN-EH** (right) in butanol. ε_{526nm} **PDIN-EH**: 120,149 M^{-1} cm^{-1} $\varepsilon_{520\ nm}$ **F-PDIN-EH**: 227,712 M^{-1} cm^{-1}.

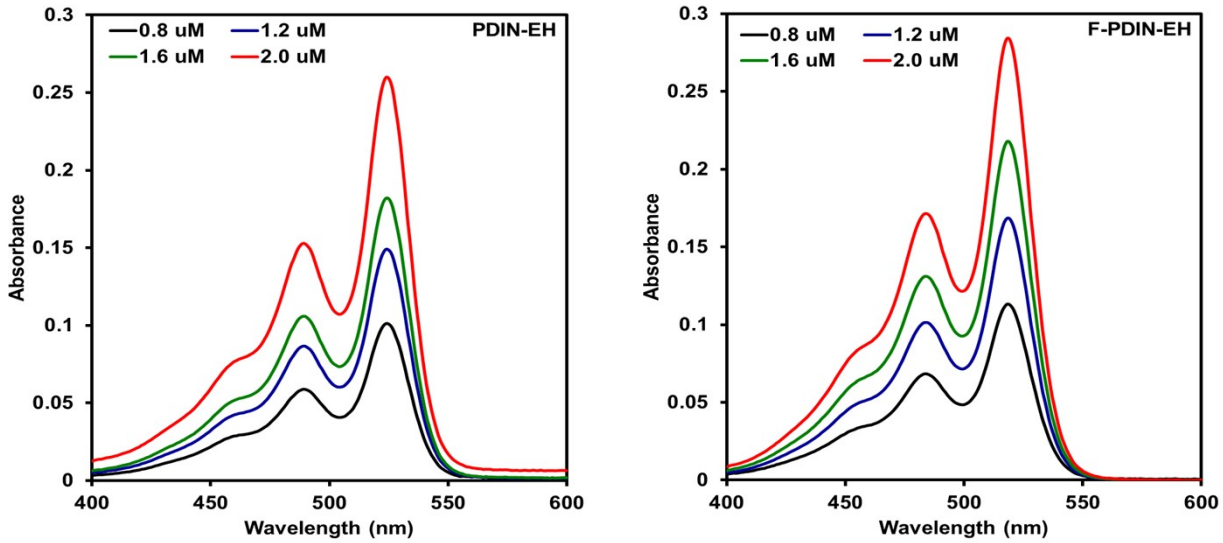

Figure S11: UV-Visible Absorption spectra for **PDIN-EH** (left) and **F-PDIN-EH** (right) material in ethanol at 0.8 to 2.0 μM concentrations taken in a 10mm pathlength quartz cuvette. λ_{max} **PDIN-EH**: 524 nm λ_{max} **F-PDIN-EH**: 518 nm.

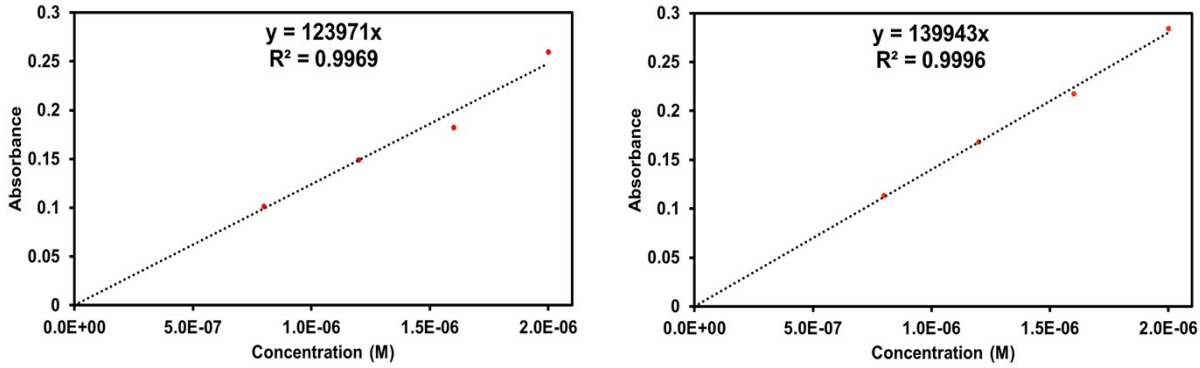

Figure S12: Absorbance vs Concentration plots for **PDIN-EH** (left) and **F-PDIN-EH** (right) in ethanol. ε_{524nm} **PDIN-EH**: 123,971 M^{-1} cm^{-1} $\varepsilon_{518\ nm}$ **F-PDIN-EH**: 139,943 M^{-1} cm^{-1}.

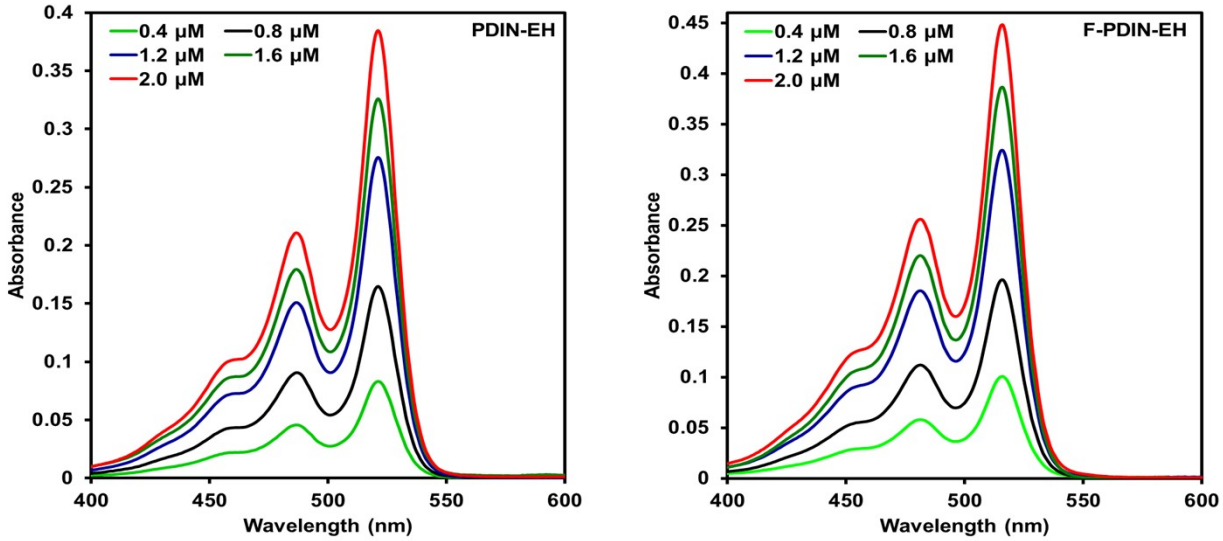

Figure S13: UV-Visible Absorption spectra of **PDIN-EH** (left) and **F-PDIN-EH** (right) material in ethyl acetate at concentrations 0.4 µM to 2.0 µM taken in a 10 mm pathlength quartz cuvette. λ_{max} **PDIN-EH**: 521 nm λ_{max} **F-PDIN-EH**: 516 nm.

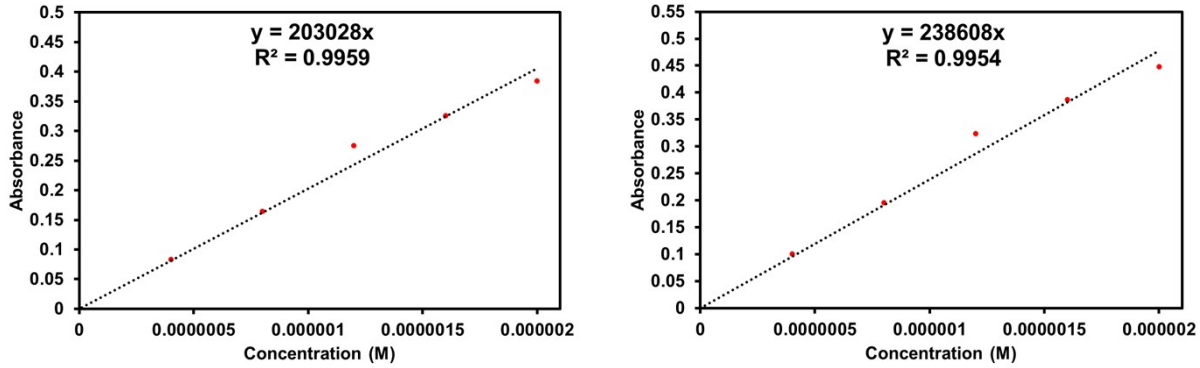

Figure S14: Absorbance vs Concentration plots for **PDIN-EH** (left) and **F-PDIN-EH** (right) in ethyl acetate. ε_{521nm} **PDIN-EH**: 203,028 M^{-1} cm^{-1} $\varepsilon_{516\,nm}$ **F-PDIN-EH**: 238,608 M^{-1} cm^{-1}.

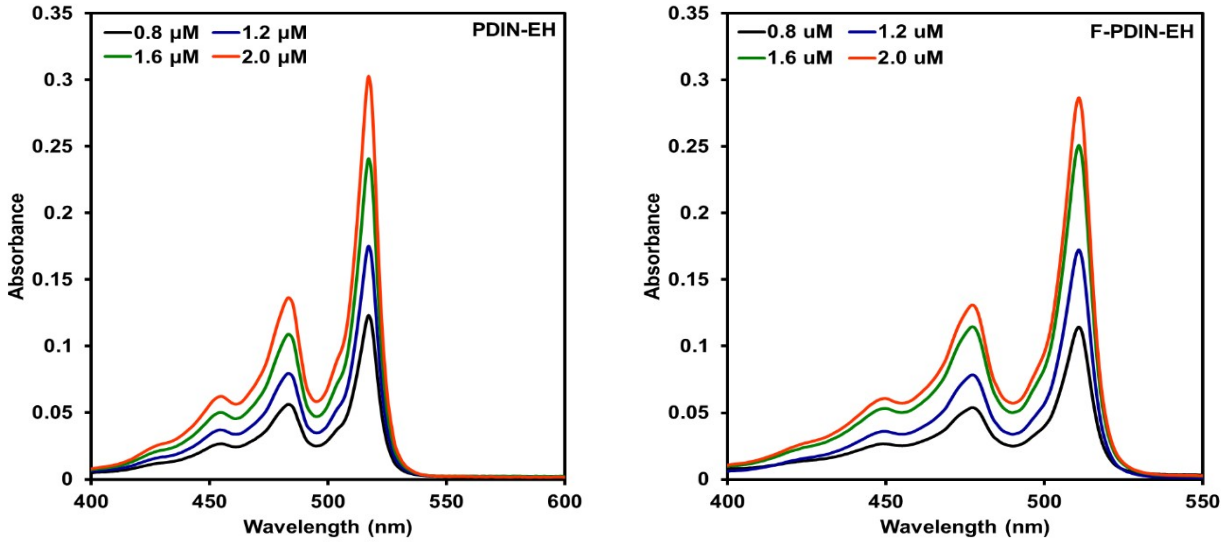

Figure S15: UV-Visible Absorption spectra of **PDIN-EH** (left) and **F-PDIN-EH** (right) material in heptane at concentrations 0.8 µM to 2.0 µM taken in a 10 mm pathlength quartz cuvette. $\lambda_{max\ \textbf{PDIN-EH}}$: 517 nm $\lambda_{max\ \textbf{F-PDIN-EH}}$: 511 nm.

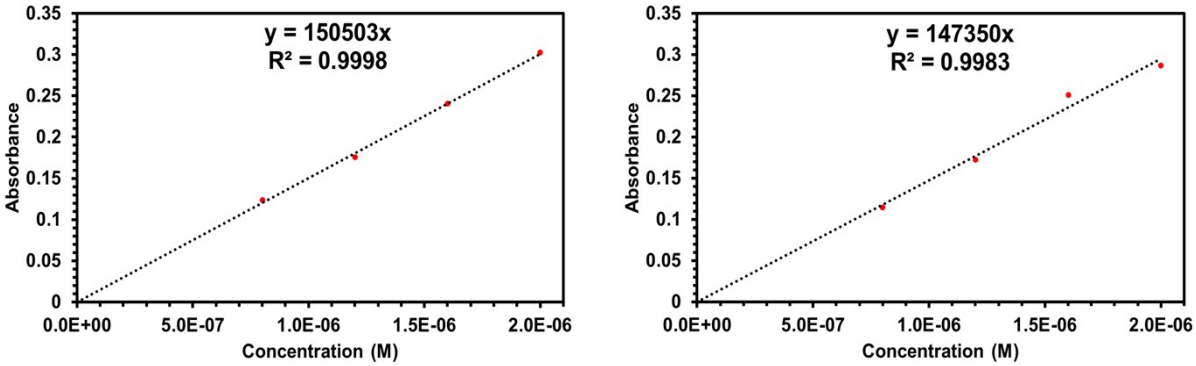

Figure S16: Absorbance vs Concentration plots for **PDIN-EH** (left) and **F-PDIN-EH** (right) in heptane. $\varepsilon_{517nm\ \textbf{PDIN-EH}}$: 150,503 M^{-1} cm^{-1} $\varepsilon_{511\ nm\ \textbf{F-PDIN-EH}}$: 147,350 M^{-1} cm^{-1}.

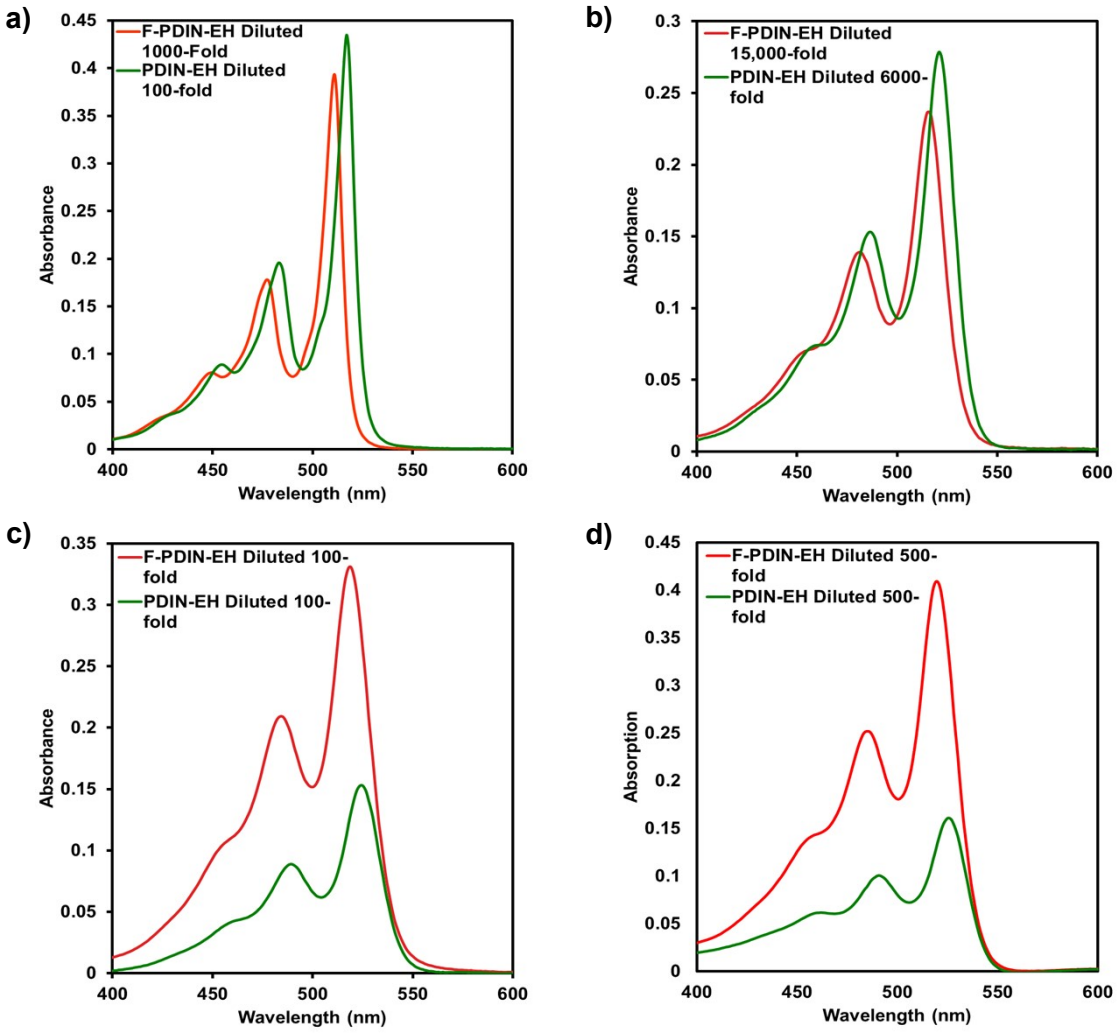

Figure S17: UV-Visible absorption spectra for diluted saturated solutions of PDIN-EH and F-PDIN-EH material in a) heptane b) ethyl acetate c) ethanol and d) butanol.

8. Solvent Interactions with Y6 NFA Blends

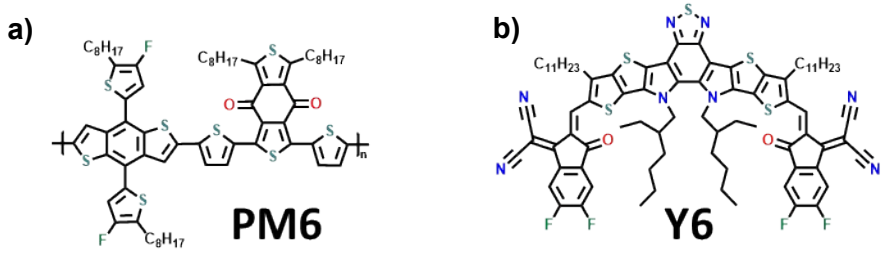

Figure S18: The chemical structures of a) polymeric donor PM6, and b) non-fullerene acceptor Y6.

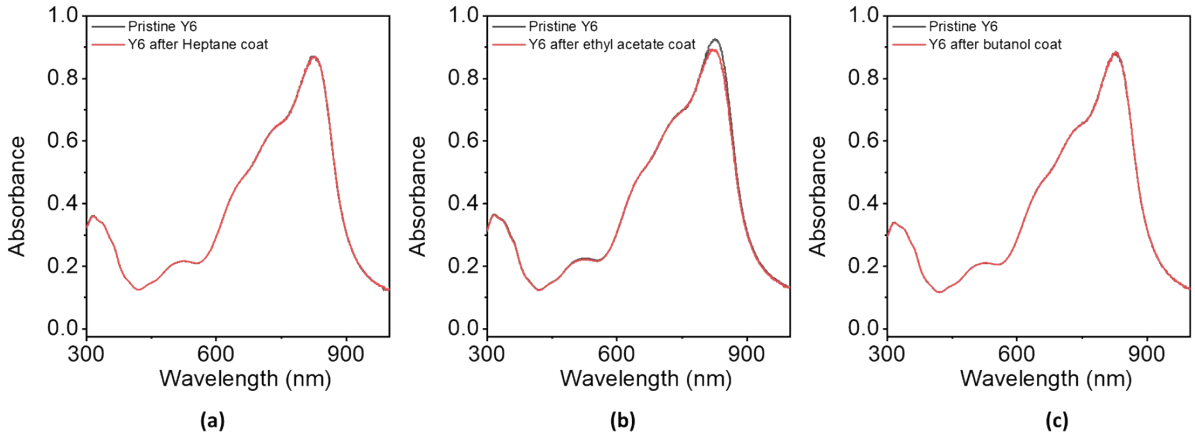

Figure S19: The UV-Vis-nearIR optical absorption spectra of the pristine Y6 films before (black) and after (red) spin coating (a) heptane, (b) ethyl acetate, and (c) butanol atop the films.

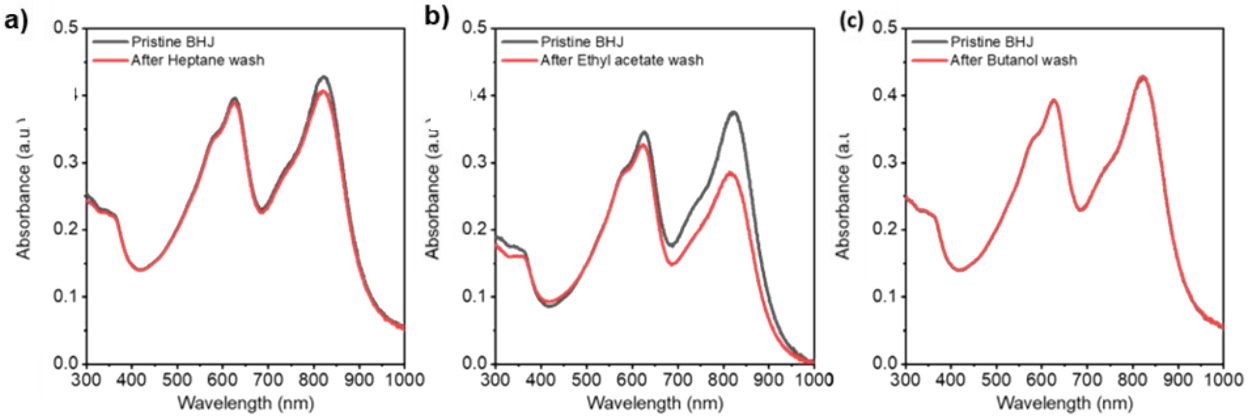

Figure S20: The UV-Vis-nearIR optical absorption spectra of the pristine BHJ films before (black) and after spin–coating (a) heptane, (b) ethyl acetate, and (c) butanol atop the films.

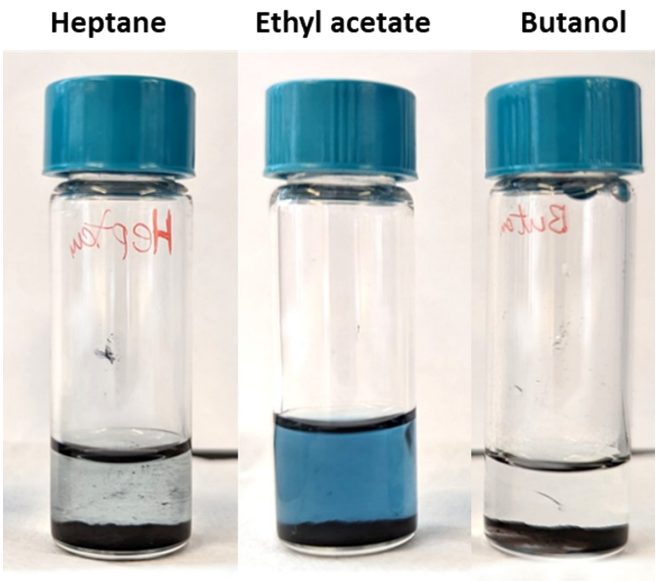

Figure S21: Picture of Y6 in heptane, ethyl acetate, and butanol at a concentration of 5.0 mg mL^{-1}.

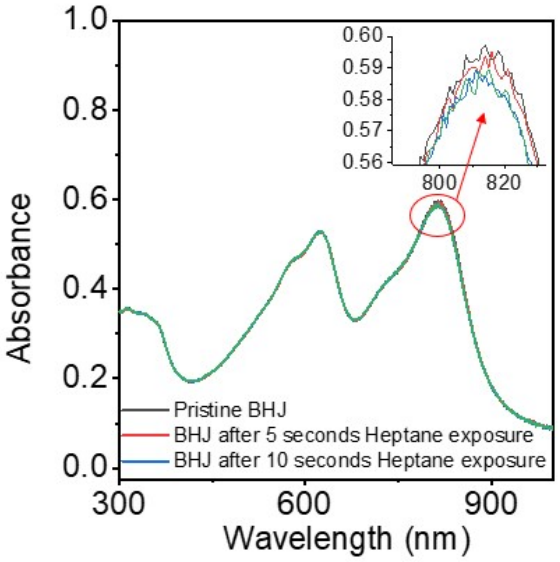

Figure S22: The UV-Vis optical absorption spectra of the PM6:Y6 BHJ films before and after coating heptane. Note: Exposure time means, the delay in coating.

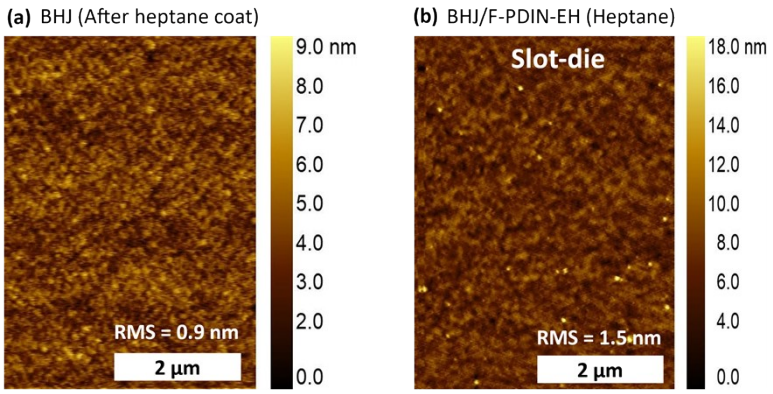

Figure S23: Atomic force microscopy height images of (a) Pristine PM6: Y6 BHJ after coating blank heptane upon the surface and (b) F-PDIN-EH atop BHJ slot-die coated from heptane.

References:

1. A. D. Hendsbee, J.-P. Sun, W. K. Law, H. Yan, I. G. Hill, D. M. Spasyuk and G. C. Welch, Chem. Mater., 2016, **28**, 7098–7109.
2. C. Song, X. Liu, X. Li, Y.-C. Wang, L. Wan, X. Sun, W. Zhang and J. Fang, *ACS Appl. Mater. Interfaces*, 2018, **10**, 14986–14992.
3. Z. He, C. Zhong, X. Huang, W.-Y. Wong, H. Wu, L. Chen, S. Su and Y. Cao, *Advanced Materials*, 2011, **23**, 4636–4643.
4. S. Lee, Y. Kim, D. Kim, D. Jeong, G.-U. Kim, J. Kim and B. J. Kim, *Macromolecules*, 2021, **54**, 7102–7112.
5. F. Pan, C. Sun, Y. Li, D. Tang, Y. Zou, X. Li, S. Bai, X. Wei, M. Lv, X. Chen and Y. Li, *Energy Environ. Sci.*, 2019, **12**, 3400–3411.
6. M. Liu, M. Li, Y. Jiang, Z. Ma, D. Liu, Z. Ren, T. P. Russell and Y. Liu, *ACS Appl. Mater. Interfaces*, 2021, **13**, 41810–41817.
7. J. Yao, S. Ding, R. Zhang, Y. Bai, Q. Zhou, L. Meng, E. Solano, J. A. Steele, M. B. J. Roeffaers, F. Gao, Z.-G. Zhang and Y. Li, *Advanced Materials*, 2022, **34**, 2203690.
8. J. Yao, B. Qiu, Z.-G. Zhang, L. Xue, R. Wang, C. Zhang, S. Chen, Q. Zhou, C. Sun, C. Yang, M. Xiao, L. Meng and Y. Li, *Nat Commun*, 2020, **11**, 2726.
9. Z. Li, X. Xu, G. Zhang, M. Deng, Y. Li and Q. Peng, *Solar RRL*, 2018, **2**, 1800182.
10. L. Liu, S. Chen, Y. Qu, X. Gao, L. Han, Z. Lin, L. Yang, W. Wang, N. Zheng, Y. Liang, Y. Tan, H. Xia and F. He, *Advanced Materials*, 2021, **33**, 2101279.
11. C. Zhao, Z. Zhang, F. Han, D. Xia, C. Xiao, J. Fang, Y. Zhang, B. Wu, S. You, Y. Wu and W. Li, *Angewandte Chemie*, 2021, **133**, 8607–8612.
12. D. Zhou, W. You, F. Yang, R. Chen, H. Xu, Y. Tong, B. Hu, L. Hu, Y. Xie and L. Chen, *ACS Appl. Mater. Interfaces*, 2021, **13**, 50187–50196.
13. C. Sun, Z. Wu, Z. Hu, J. Xiao, W. Zhao, H.-W. Li, Q.-Y. Li, S.-W. Tsang, Y.-X. Xu, K. Zhang, H.-L. Yip, J. Hou, F. Huang and Y. Cao, *Energy Environ. Sci.*, 2017, **10**, 1784–1791.
14. M. Liu, Y. Jiang, D. Liu, J. Wang, Z. Ren, T. P. Russell and Y. Liu, *ACS Energy Lett.*, 2021, **6**, 3228–3235.
15. Y. Li, M. Han, W. Yang, J. Guo, K. Chang, J. Wang, J. Min, Q. Li and Z. Li, *Mater. Chem. Front.*, 2019, **3**, 1840–1848.
16. C. Cai, J. Yao, L. Chen, Z. Yuan, Z.-G. Zhang, Y. Hu, X. Zhao, Y. Zhang, Y. Chen and Y. Li, *Angewandte Chemie International Edition*, 2021, **60**, 19053–19057.
17. Y. Li, T. Li, J. Wang, X. Zhan and Y. Lin, *Science Bulletin*, 2022, **67**, 171–177.
18. J. Han, Y. Chen, W. Chen, C. Yu, X. Song, F. Li and Y. Wang, *ACS Appl. Mater. Interfaces*, 2016, **8**, 32823–32832.
19. Q. Liao, Q. Kang, Y. Yang, C. An, B. Xu and J. Hou, *Advanced Materials*, 2020, **32**, 1906557.
20. D. Zhou, Y. Li, H. Zhang, H. Zheng, X. Shen, W. You, L. Hu, L. Han, Y. Tong and L. Chen, *Chemical Engineering Journal*, 2023, **452**, 139260.
21. W.-J. Sun, Y.-T. Wang, Y. Zhang, B. Sun, Z.-Q. Zhang, M.-J. Xiao, X.-Y. Li, Y. Huo, J. Xin, Q. Zhu, W. Ma and H.-L. Zhang, Angewandte Chemie International Edition, 2022, **61**, e202208383.
22. G. Xu, L. Gao, H. Xu, L. Huang, Y. Xie, X. Cheng, Y. Li, L. Chen and Y. Chen, J. Mater. Chem. A, 2017, **5**, 13807–13816.

23. R. Qin, D. Guo, L. Hu, Z. Liu, J. Yang, H. Liu, L. Jiang and Y. Jiang, Energy Technology, 2020, **8**, 2000072.
24. R. Peng, Z. Liu, Q. Guan, L. Hong, W. Song, Q. Wei, P. Gao, J. Huang, X. Fan, M. Wang and Z. Ge, J. Mater. Chem. A, 2018, **6**, 6327–6334.
25. Y. Liu, M. Sheri, M. D. Cole, T. Emrick and T. P. Russell, Angewandte Chemie International Edition, 2018, **57**, 9675–9678.
26. A. Hoff, A. Gasonoo, M. Pahlevani and G. C. Welch, *Solar RRL*, 2022, **6**, 2200691.
27. A. Hoff, M. Martell, A. Gasonoo, J. D. B. Koenig, P. Simón Marqués, E. Cieplechowicz, M. Pahlevani and G. C. Welch, *Advanced Engineering Materials*, **n/a**, 2201437.